JOURNAL OF GEOPHYSICAL RESEARCH, VOL. 104, NO. B5, PAGES 10,609–10,619, MAY 10, 1999

How strong is an asperity?

Charles G. Sammis

Department of Earth Sciences, University of Southern California, Los Angeles, CA.

Robert M. Nadeau and Lane R. Johnson

Center for Computational Seismology, Lawrence Berkeley Laboratory and Seismographic Station and Berkeley Seismological Laboratory, University of California, Berkeley, CA.

Abstract. A recent study of repeating earthquakes on the San Andreas Fault in central California by *Nadeau and Johnson* [1998] found that the smallest events occurred on patches having a linear dimension of the order of 0.5 m, displacements of about 2 cm, and stress drops of the order of 2000 MPa, roughly 10 times larger than rock strengths measured in the laboratory. The stress drop for larger events was observed to decrease as a power law of the seismic moment reaching the commonly observed value of 10 MPa at about magnitude 6. These large strengths are shown here to be consistent with laboratory data if the preexisting microcracks are all healed. A hierarchical fractal asperity model is presented, which is based on recent laboratory observations of contact distributions in sliding friction experiments. This "Cantor dust" model is shown to be consistent with the observed power law decrease in stress drop and increase in displacement with increasing event size. The spatial distribution of hypocenters in the Parkfield area is shown to be consistent with this simple fractal model and with a hierarchical clustering of asperities having a fractal dimension of D=1 and discrete rescaling factor of about 20.

1. Introduction

There is convincing field evidence that the San Andreas Fault (SAF) is weak in the sense that earthquakes occur at values of resolved shear stress well below those predicted by laboratory rock mechanics. Simple friction operating at lithostatic normal stress and at the observed geological displacement rates should produce a thermal anomaly that is not observed. Known popularly as the "heat flow paradox," the lack of a heat flow anomaly over the San Andreas Fault places an upper limit on the resolved shear stress of about 20 MPa [*Henyey and Wasserburg*, 1971; *Lachenbruch and McGarr*, 1990; *Lachenbruch and Sass*, 1992]. Low values of the resolved shear stress are also implied by in situ borehole measurements of stress in the vicinity of the San Andreas which find that the maximum principal stress axis is almost perpendicular to the fault plane [*Zoback et al.*, 1987].

Paradox is probably too strong a term to use here since there are at least two conceptually simple resolutions of the apparent conflict between laboratory and field strength determinations. One is the possibility that fluid pressures are very high in the fault zone. Fluid pressures approaching lithostatic pressure would reduce the effective normal stress across the fault plane to a value near zero thus allowing frictional slip at arbitrarily low values of resolved shear stress [*Rice*, 1992; *Sleep and Blandpied*, 1992; *Byerlee*, 1993]. A second possibility is that displacements normal to the fault plane during the earthquake reduce the normal stress during slip and thus lower the frictional losses. *Brune et al.* [1993], *Melosh* [1996], *Andrews and Ben-Zion* [1997], and *P. Mora and D. Place* (The dynamics of heat and earthquake faults, submitted to Journal of Geophysical Research, 1998) develop several different mechanisms through which this can be accomplished. However, none of these hydraulic or mechanical solutions has been universally accepted [see, e.g., *Scholz*, 1996].

Although the average stress drop associated with many large earthquakes is low, there may be large spatial fluctuations. Figure 1 taken from *Bouchon* [1997] is typical of many recent high-resolution images of stress drop during a large earthquake [*Beroza*, 1991; *Beroza and Spudich*, 1988; *Hartzell and Heaton*, 1983, 1986; *Antolik et al.*, 1996; *Bouchon*, 1997; *Day et al.*, 1998]. In a few small areas the stress drop exceeds 100 Mpa, while in other areas the slip leads to an increase in stress (a negative stress drop). Apparently, the fault plane is extremely heterogeneous and only accumulates stress over a small fraction of its area at a limited number of asperities. In this case, stress concentrations at the asperities can reach laboratory failure levels while the average stress over the entire fault plane depends on the fractional area of the asperities and can thus remain arbitrarily low

A recent study of repeating earthquakes on the San Andreas Fault near Parkfield California supports this picture and suggests that the stress concentrations at asperities may be even more extreme than those found in the seismic studies cited above. *Nadeau and Johnson* [1998] determined the seismic moments for 221 microearthquakes in the magnitude range -0.7 to 1.4. These earthquakes comprised 53 repeating sequences of between 2 and 13 events having essentially the same hypocenter and virtually identical seismograms. They also estimated moments for eight repeating sequences of events having magnitudes between 3.5 and 4.9 from the Stone Canyon section of the SAF originally discussed by *Ellsworth and Dietz* [1990] and for the repeating sequence of six magni-

Paper number 1999JB900006
0148-0227/99/1999JB900006$09.00

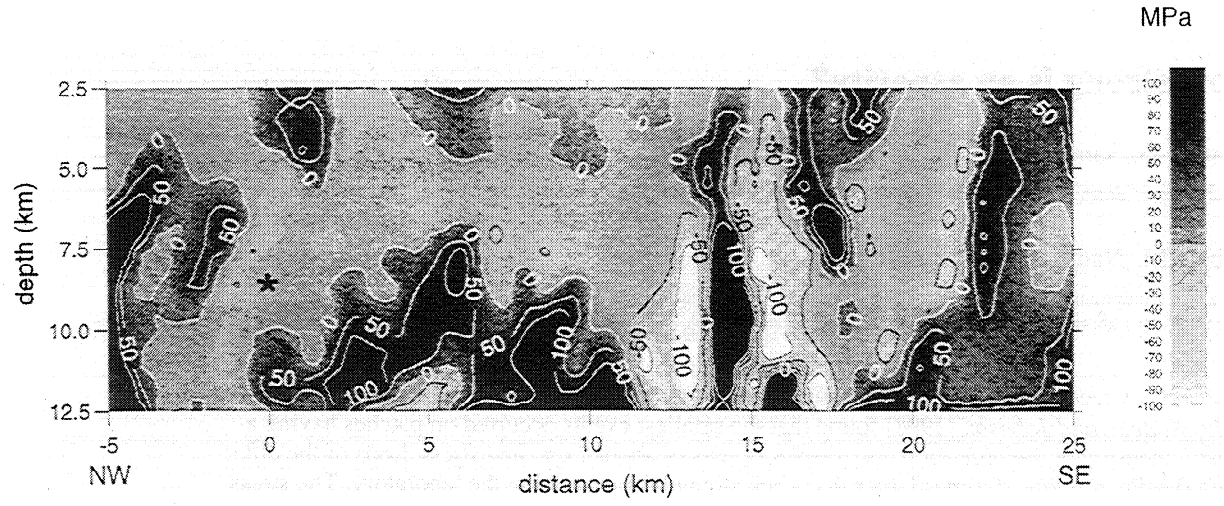

Figure 1. Tomographic image of the static stress drop inferred for the M_L =6.9 Morgan Hill earthquake from *Bouchon* [1997] calculated using the fault slip model of *Beroza and Spudich* [1988].

tude 6 events that have occurred at Parkfield since 1857 [*Bakun and McEvilly*, 1984]. The seismic moment M_0 can be interpreted in terms of the shear modulus G, the area of the rupture A, and the average displacement d as

$$M_0 = GAd \tag{1}$$

By assuming that the rate of displacement of each repeating sequence is equal to the rate of displacement for the fault segment, *Nadeau and Johnson* [1998] were able to find the area of the asperity associated with each sequence using the relation

$$\langle \dot{M}_0 \rangle = GA\langle \dot{d} \rangle \tag{2}$$

where $\langle \dot{M}_0 \rangle$ is the average rate of moment release on the repeating patch of area A and $\langle \dot{d} \rangle$ is the average slip rate on the patch which they equated with the geologically measured slip rate (2.3 cm/yr for Parkfield and Stone Canyon over the short term and 3.3 cm/yr for the larger Parkfield events over the long term). Since $\langle \dot{M}_0 \rangle$ and $\langle \dot{d} \rangle$ are known and G is easily estimated, A is determined for each repeating asperity. Knowing A for each sequence, (1) was used to find d for each sequence. Knowing d and A allowed them to estimate the stress drop, $\Delta\sigma$, for each sequence using the relation for a circular crack of radius a [see, e.g., *Kanamori and Anderson*, 1975, and references therein]

$$\Delta\sigma = \frac{7\pi}{16} G \frac{d}{a} \tag{3}$$

Nadeau and Johnson's [1998] results are consistent with the picture of a small number of very strong asperities. The smallest events occurred on patches having a linear dimension of the order of 0.5 m and a displacement of 2 cm. These large strains imply a large stress drop on the order of 2000 MPa. Larger events correspond to larger areas, but it is interesting that the displacement increases much more slowly than does the linear dimension of the fault area. Hence the faulting in these sequences is not self-similar, and stress drop decreases with increasing moment as indicated in Figure 2. However, the stress drops found for the largest repeating events at Parkfield are still between 10 and 100 times larger than those estimated for similar sized repeating events on the Calaveras Fault using the seismically derived slip duration [*Marone et al.*, 1995; *Vidale et al.*, 1994].

The observed decrease in stress drop with increasing moment suggests the possibility that larger asperities are comprised of a cluster of smaller ones such that the number of load-bearing asperities decreases with increased slip area. This picture of the stresses across a fault being supported by a small number of very strong asperities is further supported by *Nadeau and Johnson's* [1998] observation that all of the more than 6000 events recorded to date occupy less than 1% of the active fault surface. It is important to reemphasize that the high stress drops for the small events is a direct consequence of the assumption that the displacement rate for the repeating events is the same as that measured over the appropriate time interval at the surface. If shallow creep or some other mechanism is causing the surface trace to move faster than the asperities, then the stress drops calculated for the repeating events will be correspondingly reduced.

In this paper we assume that the analysis by *Nadeau and Johnson* [1998] is correct and explore two questions raised by their observations. First, are the large stress drops measured for the smallest events physically reasonable? Can rock strength reach 2000 MPa under crustal conditions as implied by their analysis? A strength of 2000 MPa is roughly 10 times that measure under crustal conditions in the laboratory. We show that such a high strength is possible if all the mechanical flaws in the rock are healed and strength is limited by true dislocation accommodated plasticity. The second question that we address is what distribution of asperities is consistent with the observed decrease in stress drop and increase in displacement with increased moment given in Figure 2? We show that a discrete hierarchical fractal distribution having a mass dimension of 1.0 is consistent with the data in Figure 2. We also show that a spatial fractal analysis of the Parkfield hypocenter data is consistent with this distribution and further implies a hierarchical fractal clustering having a discrete rescale factor near 20.

2. How Strong is Rock?

In the laboratory, rock fails by the nucleation and growth of fractures from preexisting flaws (cracks and pores). Under ten-

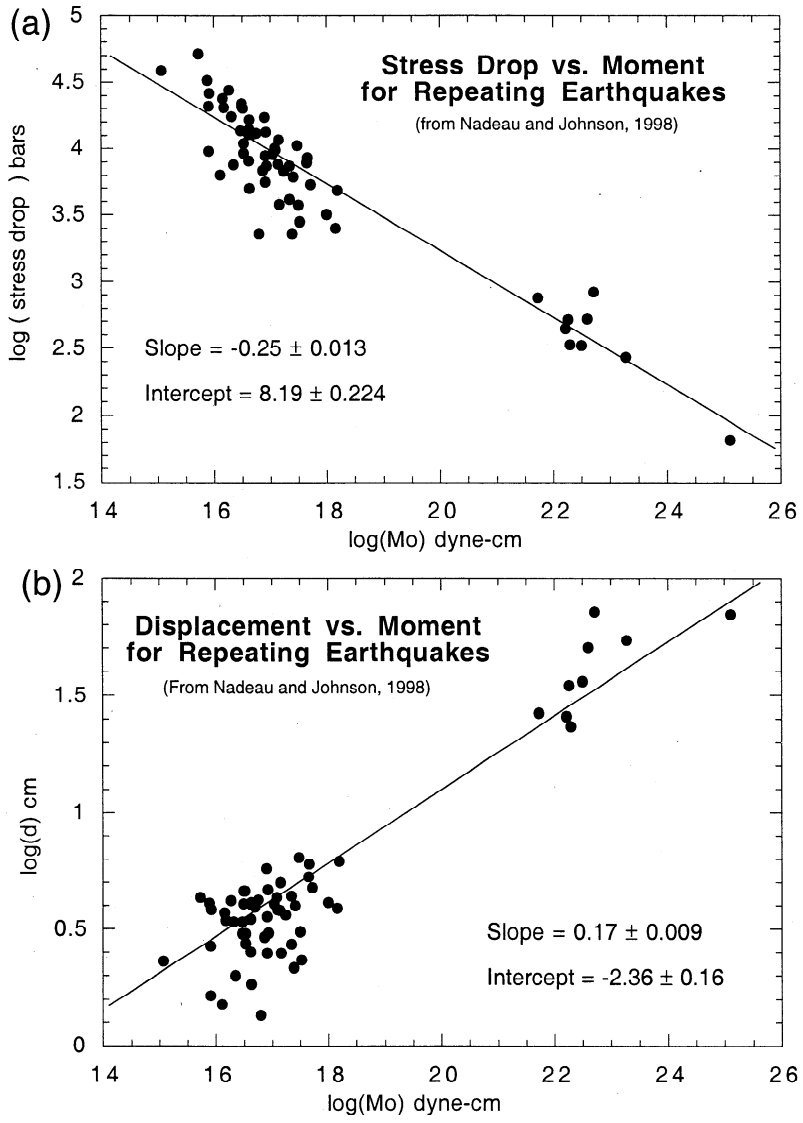

Figure 2. (a) Stress drop $\Delta\sigma$ and (b) displacement d as of function of seismic moment M_0 for repeating earthquakes on the San Andreas fault in central California [redrafted with permission from *Nadeau and Johnson*, 1998, ©1998 Seismological Society of America].

sile loading, failure occurs when the stress intensity K_I on the largest most dangerously oriented flaw reaches a critical value K_{Ic} (a material property equal to about 1 MPa $m^{1/2}$ for most ceramics).

$$K_I = \sigma\sqrt{\pi a} = K_{Ic} \tag{4}$$

where a is the half-length of the critical flaw. This is an unstable failure at constant stress since crack extension increases K_I and the critical flaw grows until it spans the sample. Under compressive loading failure is still the result of the nucleation and growth of cracks from preexisting flaws. However, in this case, crack growth is stable. Once nucleated, an individual crack requires an increase of applied stress to continue propagation. Macroscopic failure in compression is a progressive process which requires the interaction of a myriad of growing microcracks.

Ashby and Sammis [1990] formulated a damage mechanics for compressive loading based on models for the nucleation, growth, and interaction of fractures. According to their model, tensile "wing cracks" nucleate from preexisting inclined cracks of half-length a when the following conditions are met

$$\sigma_1 = \frac{\left(1+\mu^2\right)^{1/2}+\mu}{\left(1+\mu^2\right)^{1/2}-\mu}\sigma_3 + \frac{\sqrt{3}}{\left(1+\mu^2\right)^{1/2}-\mu}\frac{K_{Ic}}{\sqrt{\pi a}} \tag{5}$$

In this expression, μ is the coefficient of friction on the inclined starter flaws and σ_1 and σ_3 are the maximum and minimum principal stresses, respectively. Failure in their model is identified with the maximum value of σ_1 for a given σ_3. Up to this maximum value, crack damage is stable in that higher stress is required to produce more crack damage. Beyond the maximum the strong cooperative interaction between individual cracks causes damage to increase at decreasing values of σ_1. This is an unstable situation leading to strain localization and macroscopic failure.

It is important to note that both nucleation and failure stress scale as the square root of the initial flaw size. Universal

nucleation and failure surfaces can be expressed in terms of the dimensionless stresses

$$s_i = \frac{\sigma_i \sqrt{\pi a}}{K_{Ic}} \tag{6}$$

and crack damage is defined as

$$D = \tfrac{4}{3}\pi(l + \alpha a)^3 N_v \tag{7}$$

where l is the length of the wing crack, N_V is the number of starter cracks per unit volume, and α is a geometrical factor. In this model, the only important physical parameters that determine compressive failure strength are the size of the starter flaws and their density.

Ashby and Sammis [1990] were able to fit the failure surfaces of a number of rocks for reasonable values of μ, a and N_V. For Westerly granite, a fit to the damage initiation surface determined by *Brace et al.* [1966] and *Holcomb and Costin* [1986] and to failure surfaces measured by *Brace et al.* [1966] and *Mogi* [1966] yielded μ=0.64, $2a$=1.0 mm, and an initial damage $D_0=(4\pi/3)(\alpha a)^3 N_v=0.01$. This failure surface is shown in Figure 3 where high pressure data from *Schock and Heard* [1974] and *Shimada* [1981] have been added. Note that at confining pressures above about 200 MPa the measured failure surface deviates from the more linear theoretical surface. *Ashby and Sammis* [1990] interpreted this nonlinearity as a transition to the yield surface as the nucleation and growth of microfractures is suppressed by the high confining pressure. Similar transitions were observed in dunite, eclogite, gabbro, limestone, marble, and rock salt.

The yield surface for true plasticity is defined by

$$\sigma_y^2 = \tfrac{1}{2}\left[(\sigma_1 - \sigma_2)^2 + (\sigma_2 - \sigma_3)^2 + (\sigma_3 - \sigma_1)^2\right] \tag{8}$$

For triaxial testing conditions, $\sigma_2=\sigma_3$ and the yield surface may be reduced to $\sigma_y=\sigma_1-\sigma_3$ which is plotted in Figure 3 where the yield stress is seen to be σ_y=2600 MPa. Yield strength can be derived from hardness, H, using $\sigma_y = H/3$. For α quartz, hardness measurements give σ_y in the range 2640-3300 MPa at 0 °C and in the range 1980-2640 MPa at 300 °C [*Westbrook*, 1958]. It is characteristic of complex oxides and silicates that hardness is not temperature sensitive at temperatures up to about 0.6 of the melting temperature [*Westbrook*, 1966]. We do not therefore expect the yield strength to decrease significantly at crustal temperatures.

From Figure 3, it is apparent that laboratory confining pressures between 1000 and 2000 MPa are required to suppress microfracturing to the point where the strength is limited by plastic yielding. However, lithostatic pressure at the base of the seismogenic zone (15 km) is only about 500 MPa. Hence,

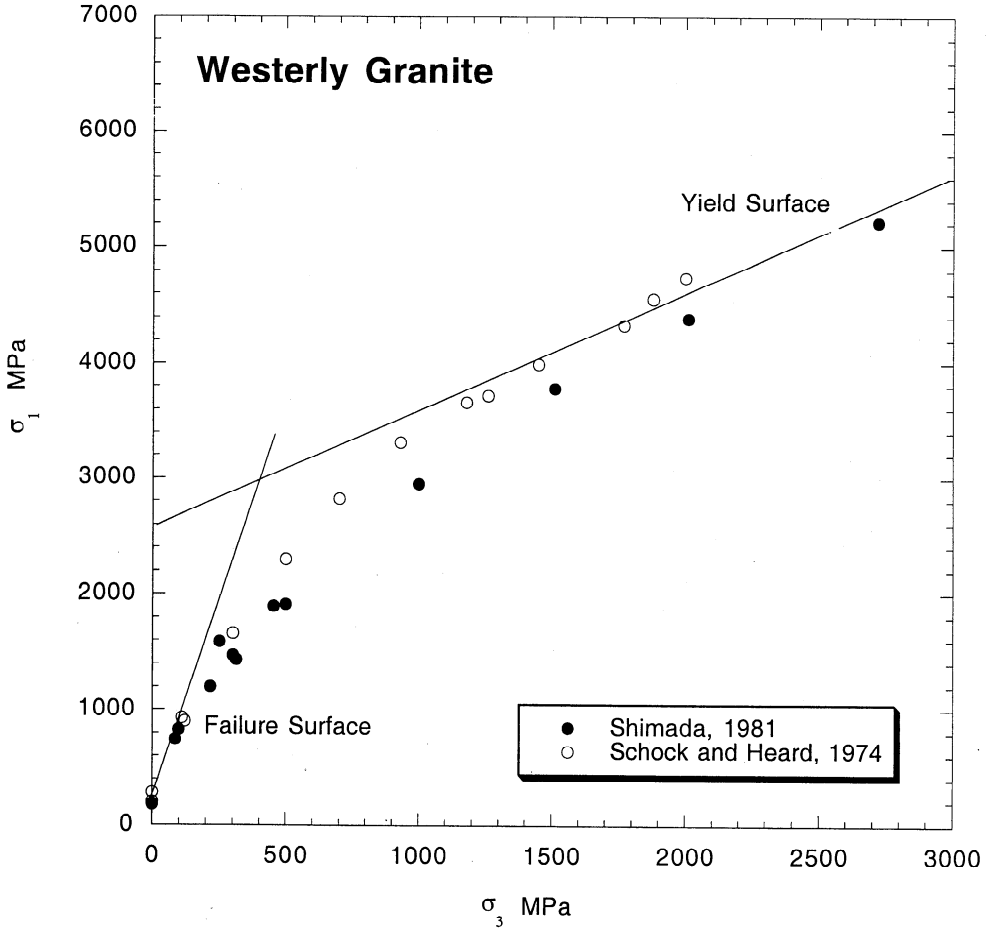

Figure 3. Failure data for Westerly granite. The failure surface was calculated using the damage mechanics model of *Ashby and Sammis* [1990]. The yield surface was calculated using experimental hardness data as discussed in the text. At large confining stress σ_3, brittle fracture is suppressed and failure occurs by plastic yielding. In the absence of microcracks, failure would occur on the yield surface at lower values of σ_3 found in the seismogenic zone thus offering a possible explanation for the high strength observed for smallest asperities.

if strength is to be limited by yielding of fault plane asperities, brittle fracture must be suppressed by some other mechanism. One possibility is the healing of preexisting flaws. Without preexisting microfractures to serve as nucleation sites, the pervasive microfracturing which leads to brittle failure cannot occur and strength will be limited by the yield surface.

So, how strong is an asperity? The maximum shear strength, $(\sigma_1-\sigma_3)/2=\sigma_y/2$ is about 1300 MPa, significantly stronger than the brittle strength under similar conditions and a bit stronger than 1033 MPa estimated for Westerly granite by *Savage et al.* [1996] using different laboratory data and a slightly different analysis.

The hypothesis that asperities fail by true plasticity implies that the stress drop should be only weakly dependent on depth because dislocation motion in the low-temperature regime (for homologous temperature, $T/T_{melting}$, less than 0.8) is relatively insensitive to pressure and to temperature. Figure 4 shows the scaled stress drop as a function of depth for the repeating earthquakes at Parkfield. The stress drop has been scaled to account for the observed decrease with increased moment in Figure 2a by plotting $[\log(\Delta\sigma)-8.19]/[-0.25\log(M_0)]$ as a function of depth. No depth dependence is evident.

Finally, if the strength of asperities is limited by plasticity, the question remains as to the nature of the instability that nucleates an event. One possibility is that the dislocation activity associated with yielding may nucleate fractures leading to brittle failure. *Ashby and Sammis* [1990] discuss evidence for this possibility in their discussion of the damage mechanics of limestone. Regardless of the mechanism responsible for the nucleation, violent failure was observed to occur up to the highest pressures shown in Figure 3. *Schock and Heard* [1974] report that their samples failed in a brittle mode at all confining pressures up to the maximum of 2010 MPa. Evidence includes a nearly linear increase of stress with strain up to failure, the audible release of strain energy upon failure, and the observation of one plane, or occasionally multiple fracture planes, with abundant slickensides.

3. Asperities and Stress Drop

The extreme strengths discussed above are only observed for the smallest events. As illustrated in Figure 2a, *Nadeau and Johnson* [1998] found that the stress drop decreases as the inverse one-fourth power of the moment

$$\Delta\sigma \propto M_0^{-1/4} \tag{9}$$

The displacement (Figure 2b) was found to be a weaker function of moment increasing with moment as

$$d \propto M_0^{0.17} \tag{10}$$

Using the basic definition of moment (1), equations (9) and (10) can be combined to give the decrease in stress drop with increasing slip area as

$$\Delta\sigma \propto A^{-0.30} \tag{11}$$

These results appear to conflict with the common observation that for larger earthquakes $\Delta\sigma$ is a constant independent of moment or area. They also do not appear to be consistent with studies of seismic radiation from small earthquakes which find that stress drop tends to decrease with decreasing moment for very small events: exactly the opposite trend to that in (9) [*Abercrombie*, 1995; *Marone et al.*, 1995; *Mayeda and Walter*, 1996; *Hardebeck and Hauksson*, 1997]. However, a decrease in stress drop with increasing moment is the expected result for a fractal distribution of asperities such as that observed by *Dieterich and Kilgore* [1996] in laboratory frictional sliding experiments. In such a fractal geometry, the density of asperities decreases with increasing slip area. This model is also supported by high-resolution spatial imaging of seismic slip during large earthquakes (cited above) which find a heterogeneous slip distribution in which isolated small areas have large slip vectors and hence stress drops which are significantly larger than the average value for the event. We show in the next section 3.1 that a fractal distribution of asperities having mass dimension $D= 1.0$ leads directly to the variation of stress drop with area found by *Nadeau and Johnson* [1998]

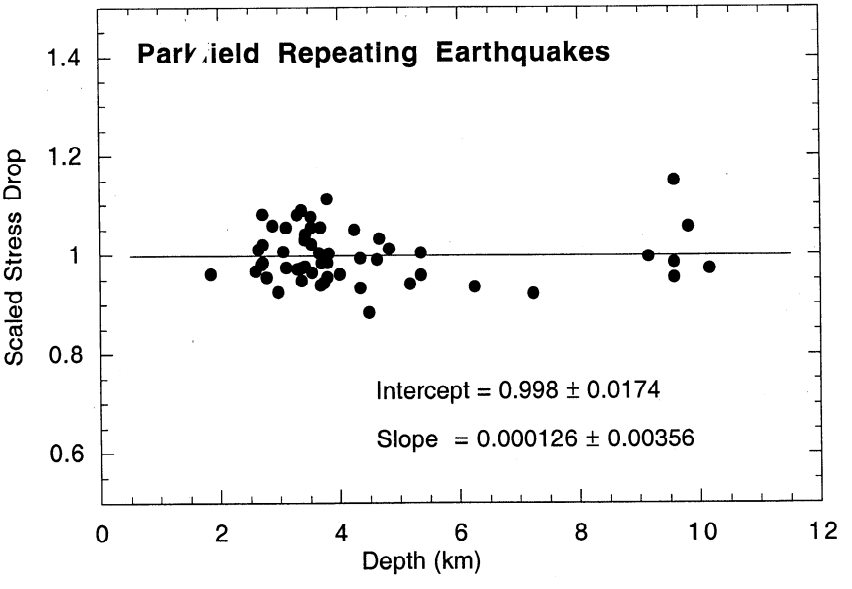

Figure 4. Scaled stress drop as a function of depth. The stress drop is scaled for moment using the dependence found in Figure 2a as scaled stress drop=$[\log(\Delta\sigma)-8.19]/[-0.25\log(M_0)]$.

in (11). The observation of constant stress drop for larger events is consistent with this fractal asperity model since the number of asperities per unit area is constant for areas larger than the upper fractal limit of the asperity distribution.

3.1. A Fractal Asperity Model

We now develop a fractal asperity model that yields the observed relation between stress drop and slip area given by (11). To begin the discussion, assume that the fault plane is populated with a distribution of unit asperities all having the same area A_0 and strength σ_0. For the smallest events, *Nadeau and Johnson* [1998] find stress drops $\Delta\sigma_0$=2000 Mpa, which we have shown is roughly consistent with the lattice shear strength of an asperity that has no unhealed flaws. This implies that the stress drop is total (i.e., $\Delta\sigma_0=\sigma_0$) for these smallest events, otherwise σ_0 would have to be larger than the intrinsic shear strength. We further assume that larger events involve the cooperative slip (possibly involving mutual triggering) of more than one unit asperity on some slipping patch of the fault. This further assumes that areas between asperities are either free to slip during an event because they bear no load or that they have already slipped in creep before the event. It is thus possible for slip on the asperities to produce a stress increase (negative stress drop) in these areas.

If a patch of fault having area A is being prevented from slipping by N unit asperities, each of which is at or just below its failure stress σ_0, then the apparent failure stress σ_f of the patch is

$$\sigma_f = \sigma_0 N\left(\frac{A_0}{A}\right) = \sigma_0 A_0 N_A \tag{12}$$

where we have defined N_A as N/A, the number of unit asperities per unit of slipping area on the fault plane. If N_A is a constant independent of A, then all patches will fail at the same stress. If the stress drop is total for all events ($\Delta\sigma=\sigma_f$), then all events will have the same stress drop, as observed for larger events but contrary to *Nadeau and Johnson's* [1998] observations for small events. However, N_A need not be constant and the stress drop need not be total.

For the following analysis, we assume that the stress drop is proportional to the failure stress on a patch and also to the displacement.

$$\Delta\sigma \propto \sigma_f\left(\frac{d}{d_0}\right) = \Delta\sigma_0 A_0 N_A\left(\frac{d}{d_0}\right) \tag{13}$$

where d_o is the displacement associated with the stress drop $\Delta\sigma_o$ when a single unit asperity fails in isolation. In general, $d>d_o$ when $A>A_o$, more than one asperity fails, and any given unit asperity may fail more than once.

Nadeau and Johnson [1998] found $d\sim M_o^{0.17}$ which, using the basic definition of moment in (1) can be written

$$d \propto A^{0.20} \tag{14}$$

Note that (11) and (14) satisfy the relation $\Delta\sigma\sim dA^{-0.5}$ as they must. If (13) is to be consistent with (11), we also require $N_A\sim A^{-0.5}$ or, equivalently,

$$N \propto A^{0.50} \tag{15}$$

The two dimensional Cantor dust in Figure 5 satisfies (15). We chose this discrete hierarchical fractal because it has a "clusters of clusters of clusters" structure which, we will show below, also characterizes the spatial structure of the seismicity at

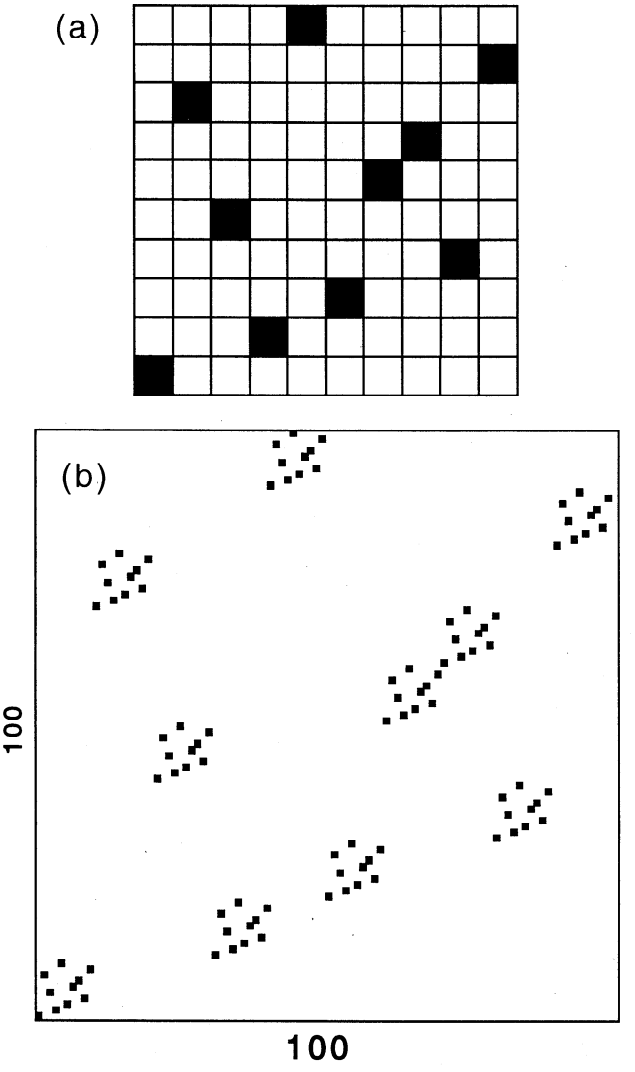

Figure 5. Two dimension Cantor dust having fractal dimension D=log10/log10=1.0. (a) The generator on a 10x10 grid and (b) the second-order figure on a 100x100 grid are shown.

Parkfield. The generator of this dust is shown in Figure 5a and two iterations of the generator are shown in Figure 5b. Since each increase in scale by a factor of 10 increases the number of asperities by a factor 10, the fractal dimension is D=log10/log10=1.0 [see *Schroeder*, 1991, chap.8]. It is more obvious that this dust has D=1 if the ten black squares in the generator are placed on the diagonal of the 10x10 matrix. Iteration of this generator produces a diagonal line at all higher orders. In fact, any generator which contains m elements on an mxm grid will have D=1 and satisfy (15). Larger grids simply produce tighter hierarchical clusters of the type in Figure 5 and thus have a larger lacunarity [see, e.g., *Turcotte*, 1997, chap.6).

The black squares in Figure 5 are taken to represent the asperities and are assumed to have unit area (A_0=1). The white areas are assumed to support no stress, either because they simply do not bear any shear load or because they creep on a timescale short in comparison to that associated with loading. In either case, stress is thereby concentrated at the asperities. If a small event ruptures one of the small (order 1) clusters of 10 asperities, then A=100. If a larger event ruptures one of the next larger (order 2) clusters of 100 asperities the correspond-

ing slipped area is 10,000. In general, for an nth order cluster, $N=10^n$ and $A=10^{2n}$ and we have $N=A^{0.5}$ as required by (15). In general, the power of A depends on the fractal dimension D of the distribution of asperities as

$$N \propto A^{D/2} \tag{16}$$

In order to get a transition to uniform stress drop for larger events, we need only require that there is an upper limit to the fractal structure above which N_A is constant. We can also ask how many orders of the fractal hierarchy in Figure 5 are required for the asperities to cover less than 1% of the fault surface as observed by *Nadeau and Johnson* [1998]. Since the asperities have unit area, we have

$$\frac{NA_0}{A} = N_A = (0.1)^n \le .01 \tag{17}$$

which has the solution $n \ge 2$.

3.2. The Spatial Structure of Parkfield Seismicity

Is there any evidence that a fractal distribution of asperities having a geometry similar to Figure 5 exists on the San Andreas Fault plane in the areas investigated by *Nadeau and Johnson* [1998]? According to the model presented above, all earthquakes should nucleate at an asperity. Even though all but the smallest events involve slip on more than one asperity, the hypocenters should correspond to the point of origin of the slip and should therefore yield a map of the unit asperities that can be analyzed for fractal structure.

Figure 6 is a hypocenter map of 1386 events on the San Anderas Fault recorded by the Parkfield array between 1987 and 1992. Even without numerical analysis, a hierarchical clustering pattern is evident in this data. One way to quantitatively characterize such clustering is the pair correlation function defined as [*Schroeder*, 1991, chap.10]

$$C(r) = \frac{N(s \le r)}{N_{\text{tot}}^2} \tag{18}$$

where $N(s \le r)$ is the number of point pairs whose Euclidean separation distance s is less than r and N_{tot} is the total number of points. The correlation dimension is then defined as

$$D_2 = \lim_{r \to 0} \frac{\log C(r)}{\log r} \tag{19}$$

In order to see how hierarchical clustering is revealed by the correlation function, we first apply it to the two-dimensional Cantor dust in Figure 5. For this analysis, the dust has been extended to order 3 (10 clusters each containing 10 subclusters each of which contains 10 asperities, all on a 1000x1000 grid). Figure 7a shows the density function $n(s)/N^2$ for this structure. The logarithm of the cumulative distribution $C(r)$ defined in (18) is plotted as a function of the logarithm of s in Figure 7b, where the slope can be seen to be $D_2 = 1.0$ as expected and the log-periodic fluctuations correspond to the

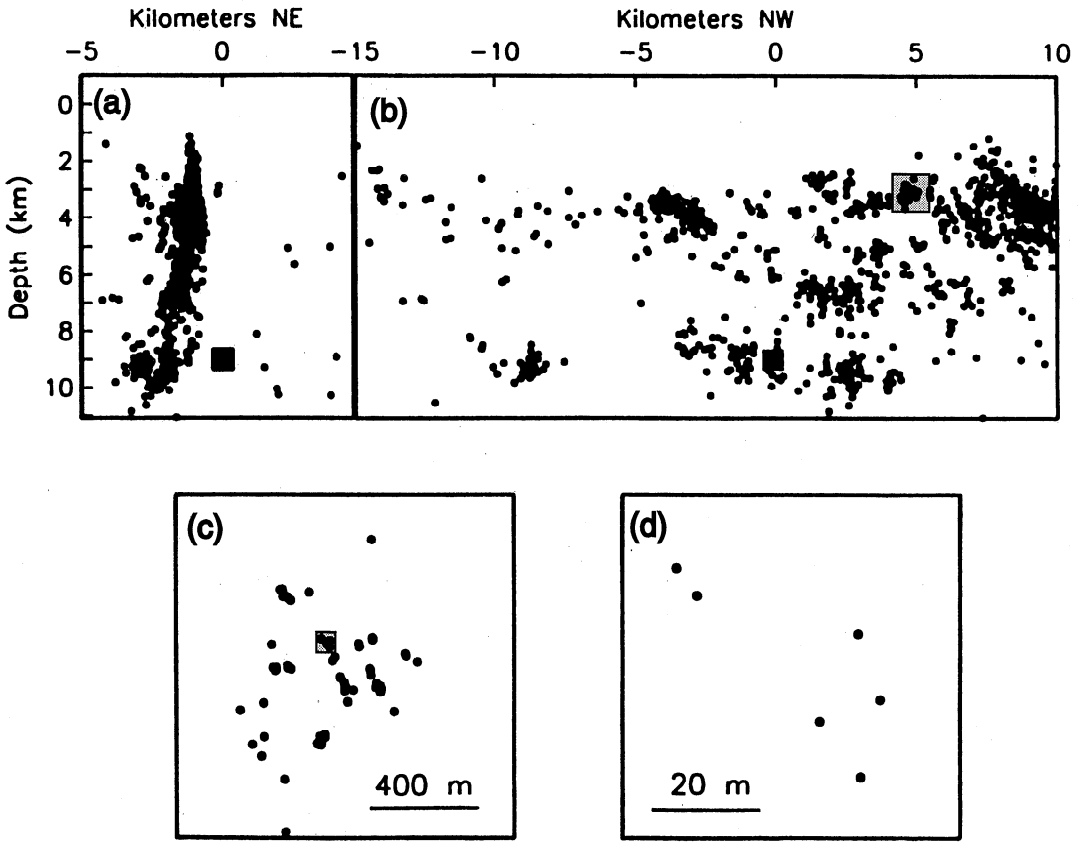

Figure 6. Hypocenter map of 1386 events on the Parkfield segment of the San Andreas Fault in central California recorded between 1987 and 1992. (a) across fault and (b) along-fault projections are shown. The square solid black symbol shows the location of the 1966 *M6* mainshock. (c) magnified area of the light grey box in Figure 6b. (d) magnified area of the light grey box in Figure 6c. Note the hierarchical structure of clusters within clusters.

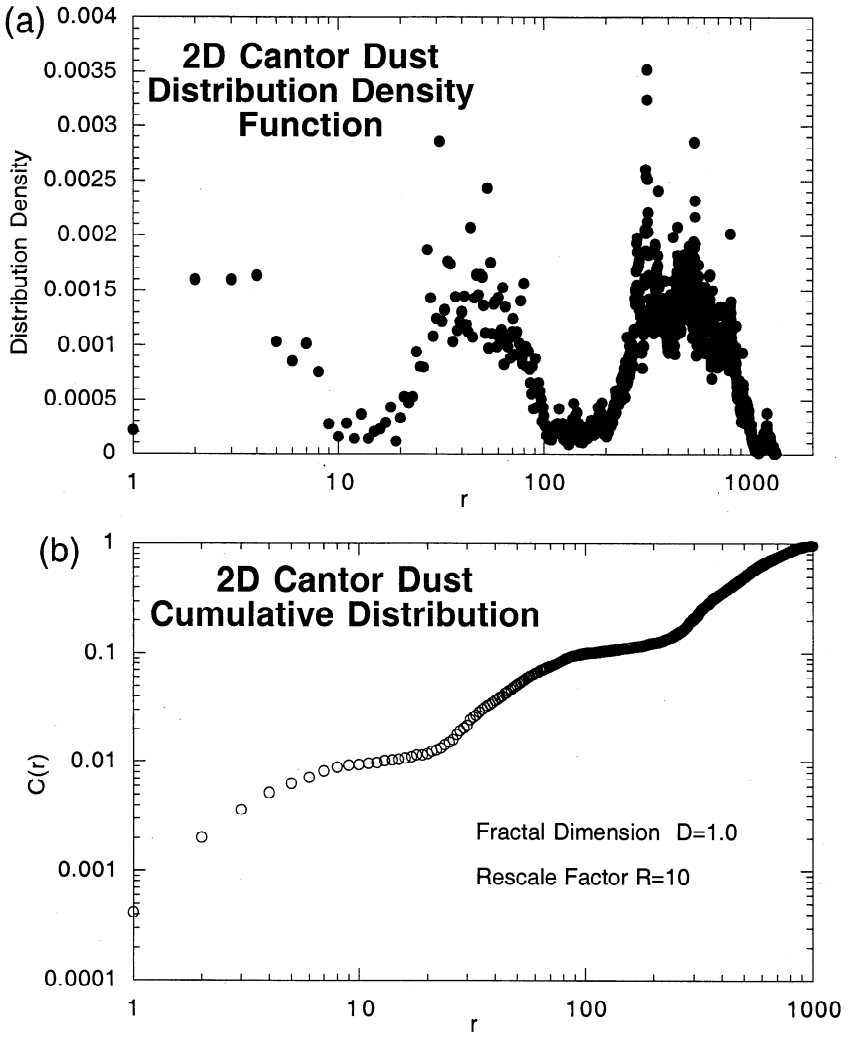

Figure 7. The pair correlation function for the Cantor dust shown in Figure 5 which has been extended to three orders on a 1000x1000 grid. (a) The density function of pair distances and (b) the cumulative distribution for which the log correlation function $C(r)$ has been plotted as a function of log$r$ is shown. The slope yields the correlation dimension D_2=1.0 . The log-periodic fluctuations yield the discrete rescale factor of 10.

three broad peaks in Figure 7a which reflect the discrete rescaling factor of 10 which characterizes this dust.

We now turn to the Parkfield seismicity data, which R.M. Nadeau and W. Foxall (manuscript in preparation, 1999) have put in a form that can be compared with the Cantor dust analysis. The procedure they used is briefly described here. All 1386 hypocenters were not located with the same accuracy. A subset of 101 events were located relative to one another such that their relative positions within clusters are accurate to about ±5-10 m and their relative positions among clusters and non-clustered events are of the order of ±20-40 m. The other events were located less precisely (±150-200 m) (see *Nadeau and McEvilly* [1997] for an analysis of the location accuracy of these data). In order that the clustering at short distances is not obscured by location error, the pair correlation function was only evaluated for each of the 101 well-located events. That is, for each of the 101 well-located events, the distance to all 1385 other events in the data set was found thus yielding 101x1385 pair distances. In a clustered hierarchy such as the Cantor dust in Figure 4, each point occupies a statistically equivalent point in the sense that $C(r)$ calculated for any given point will be essentially the same. For such a structure, the evaluation of $C(r)$ for a subset of points does not introduce a bias.

Figure 8a shows the density function $n(s)/N^2$ for the 101x1385 hypocenters pairs. Note that there are three maxima approximately equally spaced in log(s) corresponding to a rescaling factor near 20. Figure 8b shows the logarithm of the cumulative distribution $C(r)$ as a function of the logarithm of r. The corresponding correlation dimension is D_2 = 0.96, and the log-periodic fluctuations correspond to the maxima in Figure 8a. For comparison, a Cantor dust having fractal dimension D=1 and a rescale factor of 20 is shown in Figure 9. Comparison with Figure 5 shows that the larger rescale factor corresponds to tighter clustering and a larger lacunarity.

4. Discussion

We have found a discrete hierarchical fractal distribution of unit asperities which yields the observed dependence of stress drop on area and is consistent with the spatial distribution of hypocenters observed on the San Andreas Fault near Parkfield

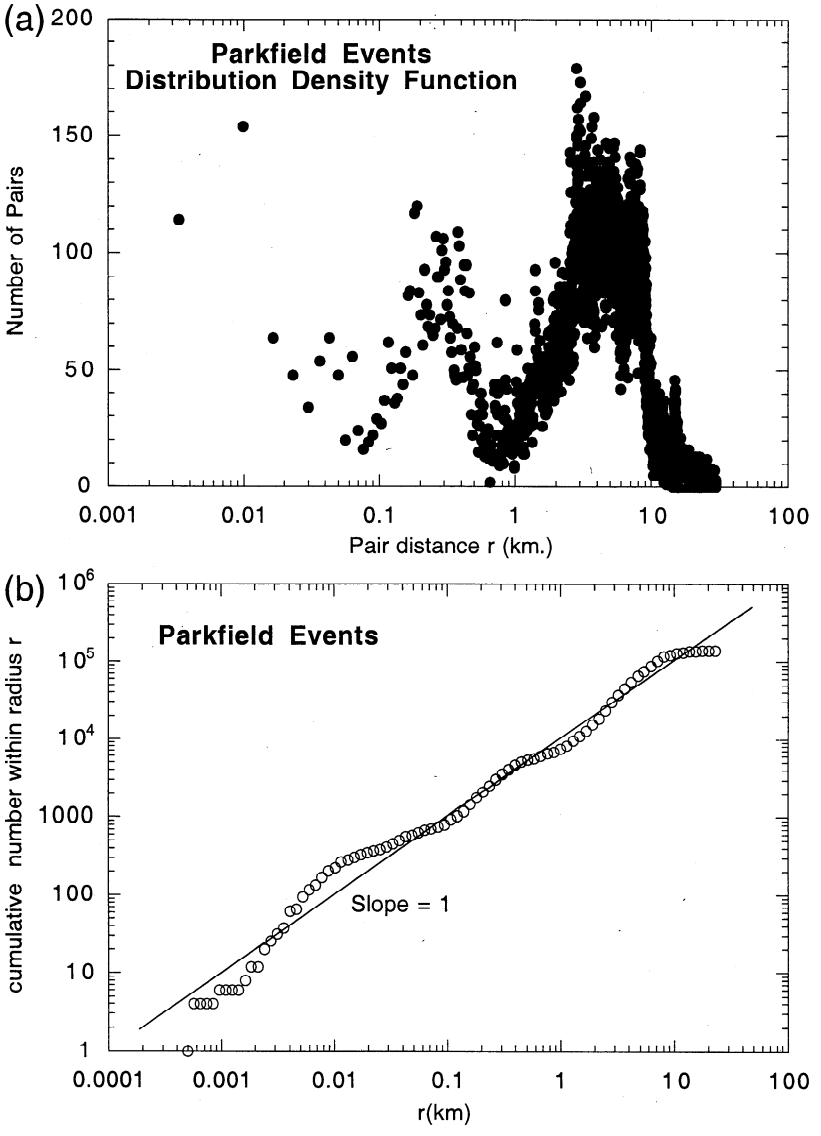

Figure 8. The pair correlation function for the Parkfield seismicity shown in Figure 6. (a) The density function of the pair distances and (b) the cumulative distribution log$C(r)$ versus log(r) is shown. The slope yields a correlation dimension of D_2=0.96. The log-periodic fluctuations correspond to the major peaks in Figure 8a and imply a discrete rescale factor of about 20.

California. For this model to explain the recent large stress drops inferred by *Nadeau and Johnson* [1998] for small events, the unit asperities must be extremely strong, having strengths 10 times those measured in the laboratory. Although we have shown that such strong asperities cannot be ruled out on physical grounds, it is not obvious that asperities can reach these strengths in the field. To do so, virtually all the microcracks would have to heal on a time short in comparison to the interseismic interval. Studies of fault zone healing in the field [*Massonnet et al.*, 1996; *Li et al*, 1998] and in the laboratory [*Karner et al.*, 1997] show that significant healing occurs under crustal conditions on the timescale of years. Microcracks in quartz heal on a timescale of a few hours at 600 °C and 200 MPa in the presence of water [*Brantley et al.*, 1990].

Fundamental questions also remain as to the origin of the hierarchical fractal structure. *Dieterich and Kilgore* [1996] found that contact between two rough random surfaces produced a fractal distribution of asperity contacts similar to the one proposed in section 3.1. The fractal dimensions of the contact distributions in their study range from near 1 to 2.7. The observed fractal dimension tended to decrease with increased contact area at higher normal stress. Although these laboratory studies offer an explanation of the fractal geometry, the physical significance of the fractal dimension D=1 or of the discrete rescaling factor of about 20 remains a mystery. One possible source of discrete rescaling is the hierarchical nested shear band structures observed in the laboratory by *Logan et al.* [1992] and in the field by *Arboleya and Engelder* [1995]. The concentration of shear into a narrow band reduces the scale of the process by a discrete factor in the range 10-100. Repeated localization within localization produces the required discrete hierarchy. How such a structure would behave mechanically is another mystery.

It is interesting that (13) alone implies a fractal dimension D=1 regardless of dependence of d and $\Delta\sigma$ on area. Since $\Delta\sigma$ must vary as $d/A^{1/2}$ dimensionally, (13) yields directly $N_A \sim A^{-0.5}$

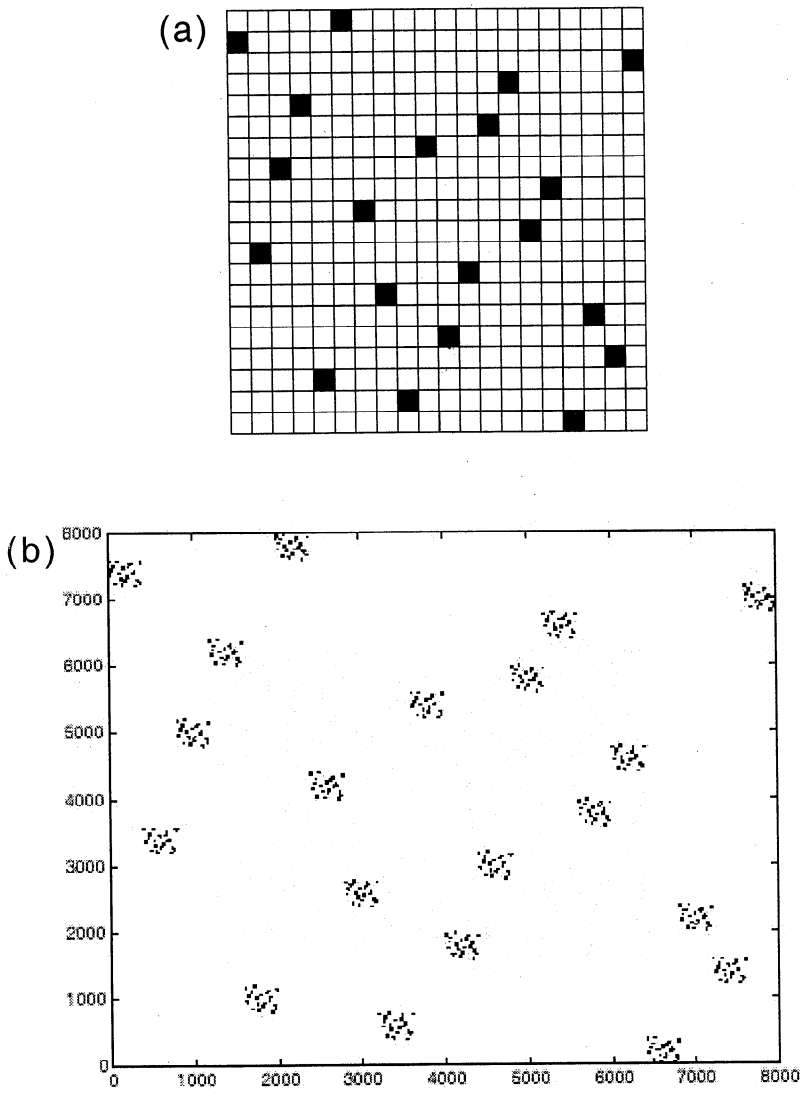

Figure 9. A Cantor dust having fractal dimension D=1 and a rescale factor of 20 comparable to the pattern of repeating earthquake hypocenters observed at Parkfield. (a) the generator is shown. (b) Three generations of the fractal on an 8000x8000 grid are also shown, although only the largest two generations can be resolved in Figure 9. Each of the smallest spots consists of the generator pattern on a 20x20 subgrid.

or, equivalently, $N \sim A^{0.5}$ which, in turn, means D=1. Hence the observation that D=1 for the Parkfield events directly supports the hierarchical clustering of unit asperities and is independent of the details of the fall off of the stress drop with increasing moment.

We also explored the possibility that the required decrease in asperity density with increasing slip area is due to clustering in a random distribution. This model also has the desired characteristic of asymptotically approaching a uniform asperity density (and hence constant stress drop) over large areas. However, the asperity density at the percolation threshold was too high to explain the decrease in stress drop with area observed by *Nadeau and Johnson* [1998].

Finally, we note that although the hierarchical geometry of asperities proposed in this paper was derived from the small repeating earthquakes studied by *Nadeau and Johnson* [1998], it is also quantitatively consistent with recent patterns of heterogeneous slip observed for larger earthquakes. Compare, for example, the stress concentrations found by *Bouchon* [1997] for the Morgan Hill earthquake in Figure 1 with the cluster pattern of small events at Parkfield in Figure 6. It is evident that the slip inversions are only resolving the first level of the hierarchy, and the stress concentrations of between 10 and 100 MPa are appropriate for this resolution based on the scaling given by (11). The implication is that improved resolution of slip will yield even higher stress drop concentrations that approach the 2000 MPa yield limit.

Acknowdedgments. We wish to thank Chris Marone, Greg Beroza, and Jim Brune for helpful comments in review and John Logan for discussions on shear localization. The Parkfield High-Resolution Seismographic Network functions through close cooperation among researchers at the University of California at Berkeley, the U.S. Geological Survey, and the Lawrence Berkeley National Laboratory (LBNL). The USGS provides primary financial support through NEHRP award 1434-95-G2540. Partial data processing was done at the Center for Computational Seismology (CCS) at LBNL, which is operated by the University of California for the U.S. Department of Energy under contract DE-AC03-76SF00098. CCS is supported by the DOE Office of Basic Energy Sciences. Support was also provided by the University of California Campus Laboratory Collaboration Project, Lawrence Livermore National Laboratory through an IGPP grant, and by the Defense Special

Weapons Agency under grant DSWA-01-97-1-0026 (LRJ) and grant DSWA-01-97-1-0005 (CGS) and by the National Science Foundation under grant EAR-9508040 (CGS).

References

Abercrombie, R.E., Earthquake source scaling relationships from -1 to 5 M_L using seismograms recorded at 2.5-km depth, *J. Geophys. Res., 100*, 24,015 - 24,036, 1995.

Andrews, D.J., and Y. Ben-Zion, Wrinkle-like slip pulses on a fault between different materials, *J. Geophys. Res., 102*, 553-571, 1997.

Antolik, M., D. Dreger, and B. Romanowicz, Finite fault source study of the great 1994 deep Bolivian earthquake, *Geophys. Res. Lett., 23*, 1589-1592, 1996.

Arboleya, M.L., and T. Engelder, Concentrated slip zones with subsidiary shears: Their development on three scales in the Cerro Brass fault zone, Appalachian valley and ridge, *J. Struct. Geol., 17*, 519-532, 1995.

Ashby, M.F., and C.G. Sammis, The damage mechanics of brittle solids in compression, *Pure Appl. Geophys., 133*, 489-521, 1990.

Bakun, W.H., and T.V. McEvilly, Recurrence models and Parkfield, California, earthquakes, *J. Geophys. Res., 89*, 3051-3058, 1984.

Beroza, C.G., Near source modeling of the Loma Prieta earthquake: Evidence for heterogeneous slip and implications for earthquake hazard, *Bull. Seismol. Soc Am., 81*, 1603-1621, 1991.

Beroza, C.G., and P. Spudich, Linearized inversion for fault rupture behavior: Application to the 1984 Morgan Hill, California, earthquake, *J. Geophys. Res., 93*, 6275-6296, 1988.

Bouchon, M., The state of stress on some faults of the San Andreas system as inferred from near-field strong motion data, *J. Geophys. Res., 102*, 11,731-11,744, 1997.

Brace, W.F., B.W. Paulding and C. Scholz, Dilatancy in the fracture of crystalline rocks, *J. Geophys. Res., 71*, 3939-3953, 1966.

Brantley, S.L., B. Evans, S.H. Hickman, and D.A. Crerar, Healing of microcracks in quartz: Implications for fluid flow, *Geology, 18*, 136-139, 1990.

Brune, J.N., S. Brown, and P.A. Johnson, Rupture mechanism and interface separation in foam rubber models of earthquakes: A possible solution to the heat flow paradox and the paradox of large overthrusts, *Tectonophysics, 218*, 59-67, 1993.

Byerlee, J.D., Model for episodic flow of high-pressure water in fault zones before earthquakes, *Geology, 21*, 303-306, 1993.

Day, S.M., G. Yu, and D.J. Wald, Dynamic stress changes during earthquake rupture, *Bull. Seismol. Soc. Am., 88*, 512-522, 1998.

Dieterich, J.H., and B.D. Kilgore, Imaging surface contacts: Power law contact distributions and contact stresses in quartz, calcite, glass, and acrylic plastic, *Tectonophysics, 256*, 219-239, 1996.

Ellsworth, W.L., and L.D. Dietz, Repeating earthquakes: Characteristics and implications, *U.S. Geol. Surv. Open File Rep., 90-98*, 226-245, 1990.

Hardebeck, J.L., and E. Hauksson, Static stress drop in the 1994 Northridge, California, aftershock sequence, *Bull. Seismol. Soc. Am., 87*, 1495-1501, 1997.

Hartzell, S.H., and T.H. Heaton, Inversion of strong ground motion and teleseismic waveform data for the fault rupture history of the 1979 Imperial Valley, California, earthquake, *Bull. Seismol. Soc. Am., 73*, 1553-1583, 1983.

Hartzell, S.H., and T.H. Heaton, Rupture history of the 1984 Morgan Hill, California, earthquake from the inversion of strong motion records, *Bull. Seismol. Soc. Am., 76*, 649-674, 1986.

Henyey, T.L., and G.J. Wasserburg, Heat flow near major strike-slip faults in central and southern California, *J. Geophys. Res., 76*, 7924-7946, 1971.

Holcomb, D.J., and L.S. Costin, Damage in brittle materials: Experimental methods, in *Proceedings of the Tenth U.S. National Congress of Applied Mechanics*, edited by J.P. Lamb, pp. 107-113, Am. Soc. Mech. Eng., New York, NY., 1986.

Kanamori, H., and D. L. Anderson, Theoretical basis of some empirical relations in seismology, *Bull Seismol. Soc. Am., 65*, 1073-1095, 1975.

Karner, S.L., C. Marone, and B. Evans, Laboratory study of fault healing and lithification in simulated fault gouge under hydrothermal conditions, *Tectonophysics, 277*, 41-55, 1997.

Lachenbruch, A.H., and A. McGarr, Stress and heat flow, *U.S. Geol. Surv. Prof. Pap. 1515*, 261-277, 1990.

Lachenbruch, A.H., and J.H. Sass, Heat flow from Cajon Pass, fault strength and tectonic implications, *J. Geophys. Res., 97*, 4995-5015, 1992.

Li, Y.-G., J.E. Vidale, K. Aki, F. Xu, and T. Burdette, Evidence of shallow fault zone strengthening after the 1992 M7.2 Landers, California, earthquake, *Science, 279*, 217-219. 1998.

Logan, J.M., C.A. Dengo, N.G. Higgs, and Z.Z. Wang, Fabric of experimental fault zones: Their development and relationship to mechanical behavior, in *Fault Mechanics and Transport Properties of Rocks*, edited by B. Evans and T.-F. Wong, pp 33-65, Academic, San Diego, Calif., 1992.

Marone, C., J.E. Vidale, and W. Ellsworth, Fault healing inferred from time dependent variations in source properties of repeating earthquakes, *Geophys. Res. Lett., 22*, 3095-3098, 1995..

Massonnet, D., W. Thatcher, and H. Vadon, Detection of postseismic fault-zone collapse following the Landers earthquake, *Nature, 382*, 612-616, 1996.

Mayeda, K., and W.R. Walter, Moment, energy, stress drop, and source spectra of western United States earthquakes from regional coda envelopes, *J. Geophys. Res., 101*, 11,195 - 11,208, 1996.

Melosh, H.J., Dynamical weakening of faults by acoustic fluidization, *Nature, 379*, 601-606, 1996.

Mogi, K., Some precise measurements of fracture strength of rocks under uniform compressive stress, *Felsmech. Ingenieurgelo., 4*, 41-55, 1966.

Nadeau, R.M., and L.R. Johnson, Seismological studies at Parkfield VI: Moment release rates and estimates of source parameters for small repeating earthquakes, *Bull. Seismol. Soc. Am., 88*, 790-814, 1998.

Nadeau, R.M., and T.V. McEvilly, Seismological studies at Parkfield V: Characteristic microearthquake sequences as fault-zone drilling targets, *Bull. Seismol. Soc. Am., 87*, 1463-1472, 1997.

Rice, J.R., Fault stress states, pore pressure distributions, and the weakness of the San Andreas Fault, in *Fault Mechanics and Transport Properties in Rocks*, edited by B. Evans and T.-F. Wong, pp.475-503, Academic, San Diego, Calif., 1992.

Savage, J.C., J.D. Byerlee, and D.A. Lockner, Is internal friction friction?, *Geophys. Res. Lett., 23*, 487-490, 1996.

Schock, R.N., and H.C. Heard, Static mechanical properties and shock loading response of granite, *J. Geophys. Res., 79*, 1662-1666, 1974.

Scholz, C., Faults without friction, *Nature, 381*, 556-557, 1996.

Schroeder, M., *Fractals, Chaos, Power Laws*, W.H. Freeman, New York, 1991.

Shimada, M., The method of compression test under high pressures in a cubic press and the strength of granite, *Tectonophysics, 72*, 343-357, 1981.

Sleep, N.H., and M.L. Blanpied, Creep, compaction, and the weak rheology of major faults, *Nature, 359*, 687-692, 1992.

Turcotte, D.L., *Fractals and Chaos in Geology and Geophysics*, 2nd ed., Cambridge Univ. Press, New York, 1997.

Vidale, J.E., W. Ellsworth, A. Cole, and C. Marone, Rutpure variation with recurrence interval in eighteen cyles of a small earthquake, *Nature, 368*, 624-626, 1994.

Westbrook, J.H., Temperature dependence of strength and brittleness of some quartz structures, *J. Am. Ceram. Soc., 41*, 433-440, 1958.

Westbrook, J.H., The temperature dependence of hardness of some common oxides, *Rev. Hautes Temp. Refract., 3*, 47-57, 1966.

Zoback, M.D., et al., New evidence on the state of stress of the San Andreas fault system, *Science, 238*, 1105-1111, 1987.

C.G. Sammis, Department of Earth Sciences, University of Southern California, Los Angeles, CA90089-0740 (email: sammis@earth.usc.edu)

L.R. Johnson and R.M. Nadeau, Center for Computational Seismology Lawrence Berkeley Laboratory and Seismographic Station and Berkeley Seismological Laboratory, University of California, Berkeley, CA 94720 (email: lrj@ccs.lbl.gov; nadeau@ccs.lbl.gov).

(Received July 1, 1998; revised December 10, 1998;
accepted December 18, 1998.)